

We are IntechOpen, the world's leading publisher of Open Access books Built by scientists, for scientists

6,900

Open access books available

185,000

International authors and editors

200M

Downloads

154

Countries delivered to

TOP 1%

most cited scientists

12.2%

Contributors from top 500 universities



WEB OF SCIENCE™

Selection of our books indexed in the Book Citation Index
in Web of Science™ Core Collection (BKCI)

Interested in publishing with us?
Contact book.department@intechopen.com

Numbers displayed above are based on latest data collected.

For more information visit www.intechopen.com



316L Stainless Steel/Hydroxyapatite Composite Materials for Biomedical Applications

Aurora Anca Poinescu and Rodica-Mariana Ion

Additional information is available at the end of the chapter

<http://dx.doi.org/10.5772/intechopen.71490>

Abstract

Hydroxyapatite (HAp) is known as one of the most important biomaterials used for orthopedic and dental applications due to chemical composition similar to that of bone and bioactive properties. However, due to its reduced resistance, HAp should be mixed with different components in order to create composite materials. A good example is austenitic stainless steel (AA 316L), as a class of metallic materials used for biomedical applications. The aim of this chapter is to show a series of our group studies for obtaining a hybrid metal-ceramic composite by powder metallurgy, the physicochemical, mechanical, and biological properties of these hybrid composites and the investigation of possible functional coating layers and adherent bioactive hydroxyapatite $\text{Ca}_{10}(\text{PO}_4)_6(\text{OH})_2$ on the metal of 316L stainless steel, correlating our data with literature data. Hardness properties of the obtained composites are close to those of human bones. In biological systems, could be observed that after 6 months, the relevant metals (Fe, Mn, Cr, and Ni) concentration (ppb), that may be released from composite materials in simulated physiological fluids (SBF), is practically zero.

Keywords: hydroxyapatite (HAp), nanotechnology, 316L, HAp thin films

1. Introduction

A definition of “biomaterial,” approved by a consensus of experts, is a nonviable material used in a device, which could interact with biological systems [1]. Except biological area, this definition covers a wide range of applications. Biocompatibility is a complex concept that considers all processes that occur in the interaction between biomaterial and a living organism. The human body is highly aggressive in terms of corrosion for proper metallic biomaterials used in the manufacture of implants. This is the reason of intensive selection of new and proper biomaterials [2].

In recent decades, several strategies have been developed to obtain biomaterials used for medical implants. The development of this field is necessary for obtaining materials with improved characteristics. Hydroxyapatite is one of the most important biomaterials used for orthopedic and dental applications due to its chemical composition like that of bone and bioactive properties [3, 4]. Austenitic stainless steels are a class of metallic materials used for biomedical applications, too. Also, 316L stainless steel has a high corrosion resistance, good mechanical properties, and relatively low cost of obtaining and processing [5].

Experimental researches in this chapter will include the following groups of materials and methods:

- Ceramics: hydroxyapatite.
- Metallic materials: 316L stainless steel.
- Composite materials HAp/316L obtained by powder metallurgy.
- Composite materials HAp/316L thin films obtained by sol-gel.
- Functional coating layers and adherent bioactive hydroxyapatite $\text{Ca}_{10}(\text{PO}_4)_6(\text{OH})_2$ on the metal of 316L stainless steel.

In this chapter the following aspects will be discussed: (i) synthesis of HAp by wet precipitation; (ii) synthesis of hydroxyapatite by sol-gel method; (iii) chemical, mechanical, and microstructural characterization of 316L stainless steel and HAp (X-ray diffraction (XRD), dynamic light scattering (DLS), Fourier transform infrared spectroscopy (FTIR), scanning electron microscopy (SEM), atomic force microscopy (AFM), mechanical (the tensile behavior, Vickers hardness, surface roughness)); (iv) synthesis and characterization of 316L steel and hydroxyapatite composites by powder metallurgy, sol-gel, and functional coating layers between both components; and (v) study of the new biomaterials behavior in simulated physiological fluids, considering that the deposition of hydroxyapatite will prevent the release of metal ions in solutions of artificial plasma and saline.

2. State of research in biomaterials

2.1. Preparation of hydroxyapatite by wet chemical precipitation method

This method is easy to achieve, at low temperature, with relatively high percentage of pure product and with not very expensive equipments [6, 7].

Hydroxyapatite could be obtained by chemical precipitation method modified by Sung [8]. Commercial chemical reagents used are calcium nitrate tetrahydrate $\text{Ca}(\text{NO}_3)_2 \cdot 4\text{H}_2\text{O}$ and ammonium dihydrogen phosphate $(\text{NH}_4)_2\text{HPO}_4$, separately dissolved in distilled water with stirring. After addition of $\text{Ca}(\text{NO}_3)_2$ in aqueous solution over the $(\text{NH}_4)_2\text{HPO}_4$ and shaken at room temperature for about 1 h, a milky precipitate, somewhat gelatinous, has been obtained

which in turn was stirred for 1 h for a perfect mixing [9, 10]. The mixture thus obtained was sintered at 100°C for 24 h. After that the precipitate was washed and filtered on a glass filter. After filtration, sticky compacted product was dried in an oven at 80°C. Then, dry powder was crushed in a mortar and pestle and then calcinated in a crucible of alumina at three different temperatures: 800, 1000, and 1200°C for 1 h.

The best results have been obtained at a temperature of 1000°C, at the same molar concentrations and the same method of refluxing.

The samples calcinated at different temperatures (850, 1000, and 1200°C) were analyzed by spectral techniques: X-ray diffraction (XRD), Fourier transform infrared spectroscopy (FTIR), Raman spectroscopy, dynamic light scattering (DLS), scanning electron microscopy with energy-dispersive spectroscopy (SEM-EDS), and atomic force microscopy (AFM).

The powder synthesized chemically is consistent with diffraction reference ASTM pure HAp [11, 12]. Identification of phases identified in the synthesized hydroxyapatite allow the network parameters calculation by setting 2θ . For this purpose, it has been taken into account the width of diffraction peaks at half height of them, the lines having hkl indices (200), (002), (102), (210), (310), and (004), in accordance with literature data [13, 14].

The most intense peaks appear in 2θ between 20° and 60°. X-ray diffraction data by peak characteristic (002), (211), (112), and (300) showed a high degree of purity of hydroxyapatite (**Figure 1**). This is confirmed by X-ray diffraction that shows the results are obtained in good agreement with literature data [11, 15],

These data are completed with the FTIR data, the best results being obtained for powder calcined at 1000°C [16]. The ion stretching vibration around 3568 cm⁻¹ confirms the presence of a hydroxyl group. It should be noted that the hydroxyapatite sample (HAp1) calcinated at 800°C contains water of crystallization and hydration, the HAp2 sample subjected to calcination at 1000°C has a decreased water content, and the HAp3 sample calcinated at 1200°C contained a higher water content than HAp1 due to high reactivity of the powder [17].

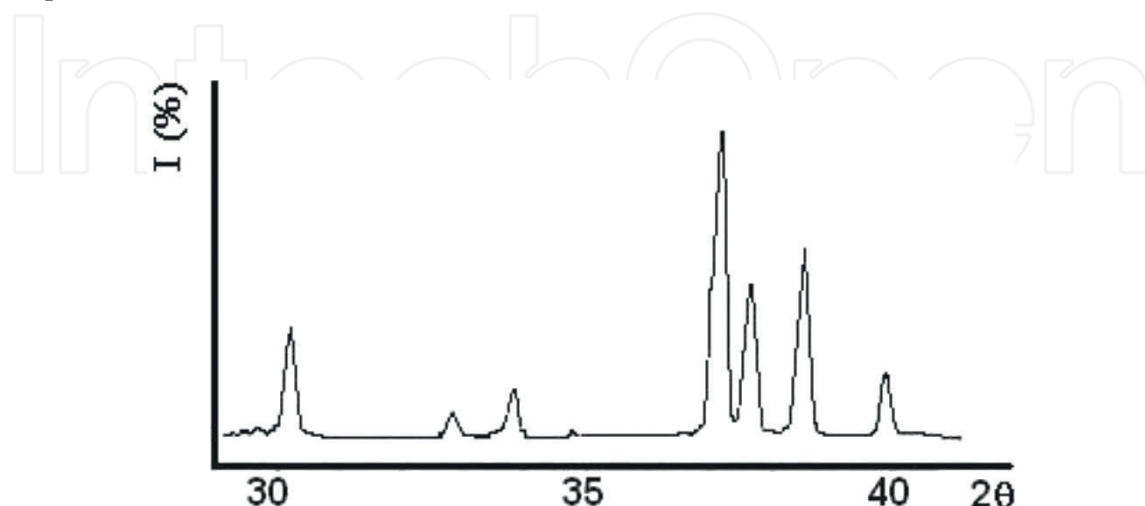


Figure 1. X-ray diffraction peaks for HAp powder 2, calcined at 1000°C, 1 h.

Likewise, the other stretching vibrations for carbonyl and phosphate groups were also observed as reported earlier [18, 19]. The broad absorption band from 1050 cm^{-1} is an evidence for tricalcium phosphate as reaction product. Literature studies indicate that tricalcium phosphate is present over 850°C . **Figure 2** showed the three FTIR curves performed on three types of hydroxyapatite, calcined at temperatures of 800, 1000, and 1200°C , respectively. FTIR tests revealed the role of hydrogen and -OH group in the hydroxyapatite samples, and the only band that differentiate these three samples is the intense band from 1624.7 cm^{-1} .

Dynamic light scattering is a well-established, versatile, and noninvasive technique which can provide information about the size distribution of the particle populations in real time. DLS data provide information about the size distribution of the HAp crystals and their concentrations in aqueous solutions that is not available from other techniques [20]. It has also been extensively used to examine the sample homogeneity. The dynamic light scattering experiment shows that the particle size distribution is in the range of 50–70 nm, which is well supported by other techniques. Dynamic light scattering is used to monitor the size of the precipitating particles and to provide information about their concentration, including different associations in different orders, which generates large aggregates (**Figure 3**).

Structural characterization of hydroxyapatite powders calcinated at 1000°C was performed by scanning electron microscopy (SEM) and atomic force microscopy (AFM), too, for analyzing the morphology and particle size. In the SEM images some small crystallites of

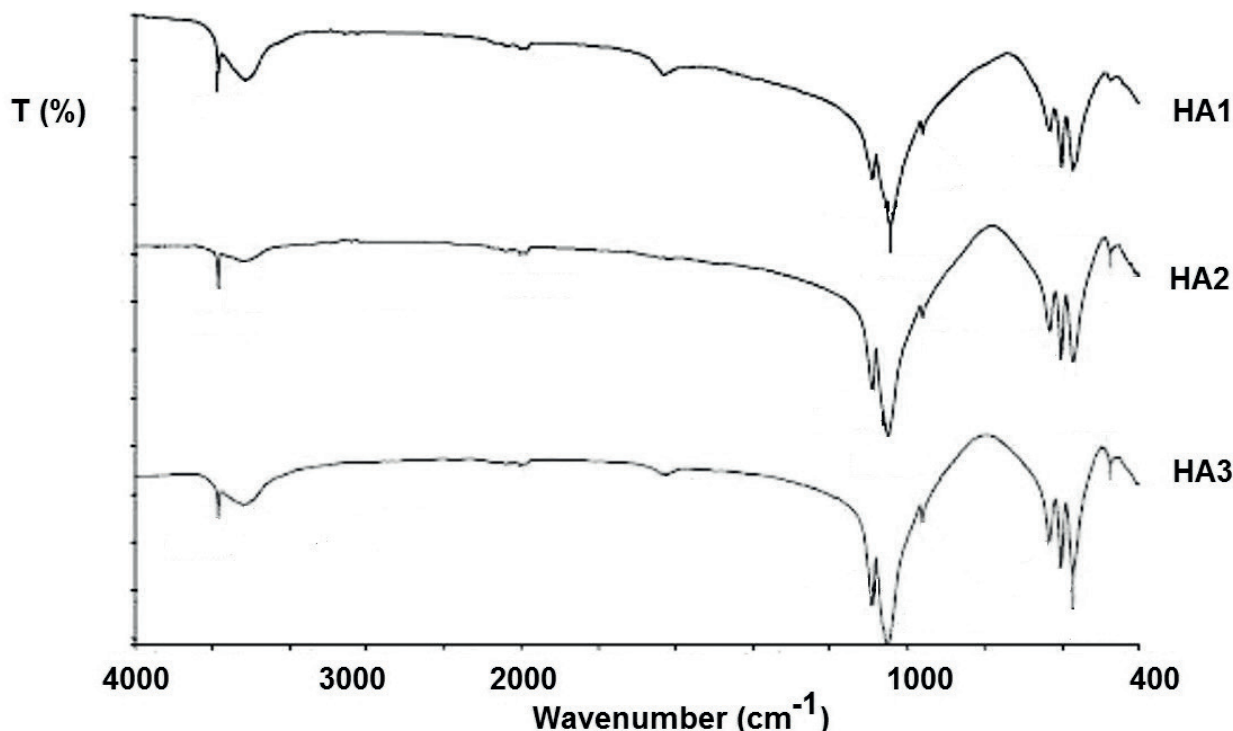


Figure 2. FTIR curves performed of hydroxyapatite, calcined at temperatures of 800, 1000, and 1200°C .

hydroxyapatite ($<100\text{ nm}$) and agglomerated particles are distinguished. Crystallites have uniform sizes with narrow particle size distribution.

The hydroxyapatite powder obtained by wet precipitation calcinated at 1000°C has been characterized by scanning electron microscopy. **Figure 4** presents scanning electron microscopy of hydroxyapatite sample calcined at 1000°C with a magnification of $2000\times$, and in **Figure 5**, it presents the same sample but at a magnification of $1000\times$. We can distinguish microporosity ($<10\text{ }\mu\text{m}$), allowing diffusion of ions and fluid from macroporosity ($100\text{--}600\mu\text{m}$) and can promote cell colonization.

To investigate with the atomic force microscope, hydroxyapatite solutions were freshly prepared before each experiment, by suspending an appropriate amount of each sample in ethanol. Compared with existing literature data [20], hydroxyapatite has a y -plane orientation. In our experiments, it can be observed that the grain is oriented occurring after z -plane.

By atomic force microscopy investigations, it was found that hydroxyapatite from bulk phase, at higher calcination temperatures, is agglomerated in nanoparticle phase and then in nanocrystalline spherule forms. Crystal size distribution depends on the critical size of nuclei in saturation conditions rather than the crystal growth if clusters of small particles are observed in AFM images.

In conclusion, hydrothermal synthesis method applied to HAp leads to the hydroxyapatite powders with a nanocrystalline of high and good stoichiometry, with a relatively narrow distribution of crystal size. Also, at high calcination temperature and long-term (4 h) of treatment, well-crystallized products were obtained, with desired parameters [21].

AFM technique has been used for evaluation the distribution of high spherules, visible in HAp powder [21]. The AFM method revealed a rugged HAp surface with crystallites ranging from 70 to 100 nm in accordance with other spectral methods. It has been found that at higher calcinations of temperatures HAp is deagglomerated from the bulk phase and agglomerates

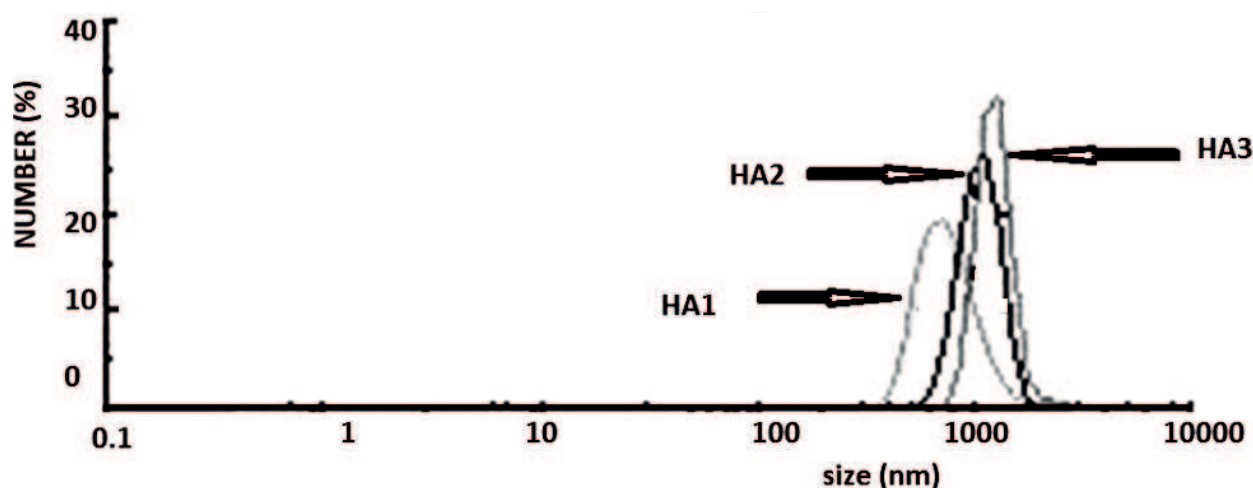


Figure 3. Particle size distribution of the three records by number.

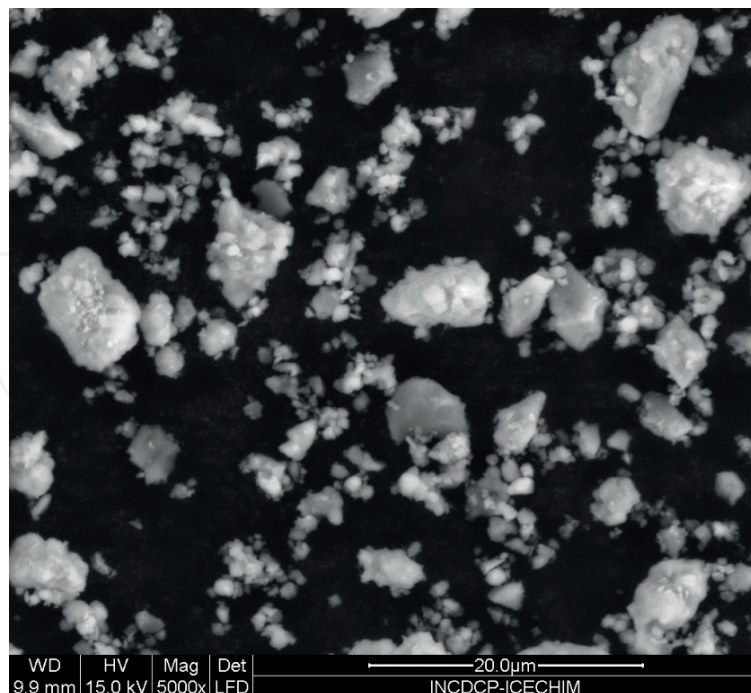


Figure 4. Scanning electron microscopy of HAp powder calcined at 1000°C, 5000×.

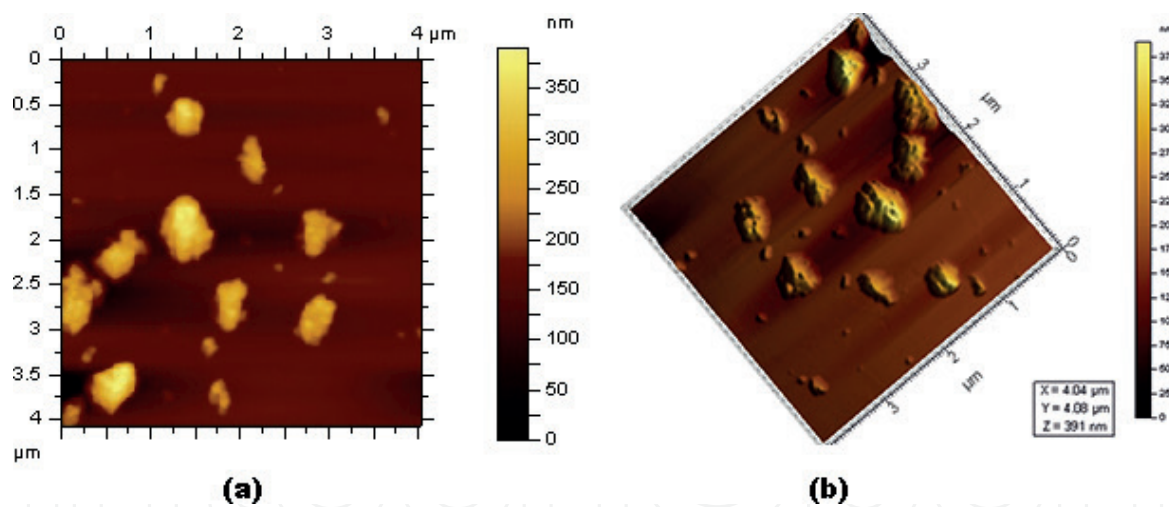


Figure 5. 3D representation of the grains of calcined hydroxyapatite at 1000°C.

in the nanoparticle phase that results in the formation of nanocrystalline and then spherules. The AFM 3D topography of hydroxyapatite powder was recorded on an area of $5 \times 5 \mu\text{m}^2$, **Figure 5 (a,b)**.

The crystal size distribution depends on the critical dimensions of the nuclei under oversaturation conditions rather than on the crystal growth if particle agglomerations are observed.

2.2. Sol-gel method

The precursors used to prepare hydroxyapatite were calcium nitrate tetrahydrate $\text{Ca}(\text{NO}_3)_2 \cdot 4\text{H}_2\text{O}$ and phosphorus pentoxide (P_2O_5) (Chimreactiv, Romania). To a solution of 0.5 mol/l, phosphorus pentoxide (P_2O_5) was dissolved in ethanol. $\text{Ca}(\text{NO}_3)_2 \cdot 4\text{H}_2\text{O}$ was also dissolved in absolute ethanol to form a solution of 1.67 mol/l mixing both solutions were constantly stirred with a magnetic stirrer, after which the mixture was placed in an oven at an 80°C temperature for 24 h to complete the reaction [22, 23]. Dried gel was performed in an oven. The resulting product was a transparent gel. The samples were heat treated to transform the acid gel into a solid product with properties of biocompatibility and osteoconductivity

Before depositing onto 316L stainless steel, the hydroxyapatite film has been characterized by X-ray diffraction, and the results were relevant in terms of purity and presence of this compound. After analyzing, the diffraction phases identified in hydroxyapatite obtained by sol-gel were hydroxyapatite $(\text{Ca})_{10}(\text{PO}_4)_6(\text{OH})_2$ and tricalcium phosphate $\text{Ca}_3(\text{PO}_4)_2$. X-ray diffraction analysis reveals a high degree of crystallinity for HAp obtained by sol-gel. A broad reflection peak appears in the range of 31.8–32.51 2Θ , which represents the characteristic peak of apatitic phase (according to JCPDS card #9-432). Some characteristic peaks at, for instance, (211), (300), and (212) planes were shown for coatings annealed at higher temperatures 400–500°C. This suggests that the apatite coatings with structural evolution from amorphous to crystalline are able to produce depending on the temperatures.

3. HAp:316L composite materials

3.1. Composite HAp:316L obtained by cold pressing

Three technological versions of biocomposites obtained by powder metallurgy have been prepared by cold pressing, by varying the bulk concentrations [17, 18]. There have been five series of powder mixtures:

- Hydroxyapatite:316L stainless steel = 80%:20%.
- Hydroxyapatite:316L stainless steel = 50%:50%.
- Hydroxyapatite:316L stainless steel = 30%:70%.
- Hydroxyapatite:316L stainless steel = 20%:20%.

Quantitative measurement of the diameters of 316L powder particles was performed from SEM images. **Figure 6** shows SEM micrography of 316L stainless steel powder, and the size of powder varies between 142 and 195 μm . Powders are spherical slightly dendritic. There is a considerable disparity in both powder sizes which could lead to segregation during compaction, thus providing a compact product heterogeneity. One of the most important problems in



Figure 6. Scanning electron microscopy (500 \times).

the compaction process and its efficiency is given by applied powder shape. Hydroxyapatite powder is spherical, while the steel powder is dendritic in good agreement with literature's report [24, 25].

3.1.1. HAp:316L composite (80% HAp:20% 316L)

80% hydroxyapatite powder and 20% 316L stainless steel powder were mixed, were homogenized, and after which they were cold uniaxially pressed. The samples were sintered at 850 and 1000°C, held for 60 and 120 min. Sintering process took place in a protective atmosphere of H₂ with a cooling and heating at rate of 10°C/min (**Figure 7**).



Figure 7. Visual aspect of sample 2, 850°C, 120 min.

Macroscopic characterization of all four samples indicates a high porosity, exfoliation, and friability. Without lubricant for pressing, to avoid contamination with toxic material, a poor compaction of materials and a high porosity of the tablet are observed.

3.1.2. *HAp:316L composite (50% HAp:50% 316L)*

The material obtained by mixing powder of 50% 316L and 50% HAp was cut along the atomic planes. Material destruction was caused by different granulations of the two sorts of particles (too small for hydroxyapatite fraction $<45\text{ }\mu\text{m}$), the manual mixing and different densities ($\rho_{\text{HAp}} = 1.5\text{ g/cm}^3$; $\rho_{\text{316L}} = 3.0\text{ g/cm}^3$), of the two materials.

3.1.3. *HAp:316L composite (70% 316L:30%HAp)*

The preparation procedure of these composites was similar to the previous work on the same parameters. Fractions chosen for powder mixtures 70:30 were $>160\text{ }\mu\text{m}$ for stainless steel 316L and $>45\text{ }\mu\text{m}$ for hydroxyapatite. Three composite samples with cylinder shape have been obtained.

The SEM image of the obtained composite *HAp:316L composite (70% 316L:30%HAp)*, **Figure 8**. A relatively uniform distribution of stainless steel powder can be explained by mixing two types of powders performed manually. The metal particles looks as white formations, round, slightly dendritic, meanwhile the hydroxyapatite particles become dark coloured.

EDAX analysis of the composite with 70% 316L and 30% HAp is shown in **Figure 9**; the presence of phosphorus and calcium from hydroxyapatite and the presence of elements such as Ni, Cu, Cr, and Fe as specific metal elements of 316 stainless steel could be observed.

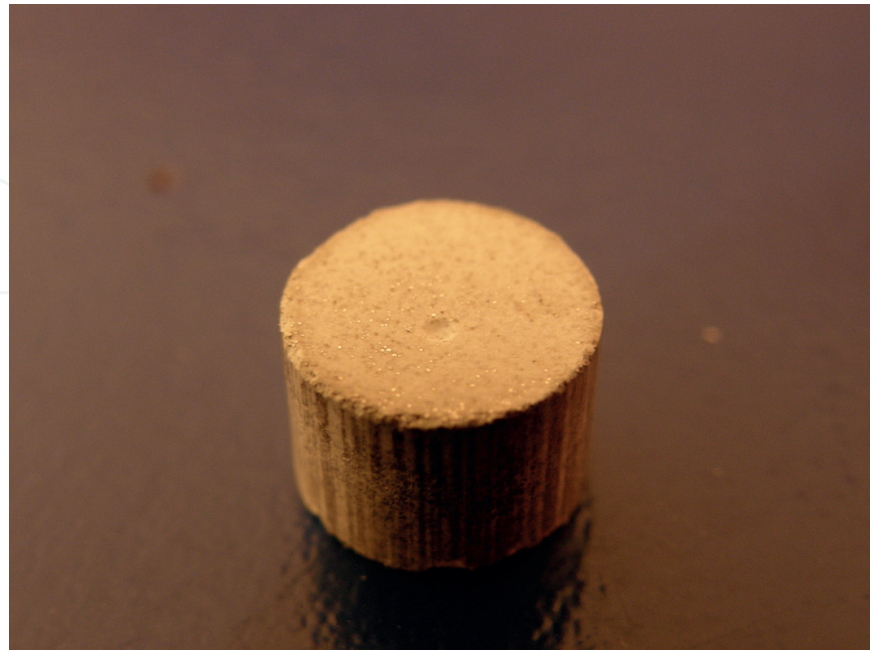


Figure 8. Composite image 70% 316L and 30% HAp.

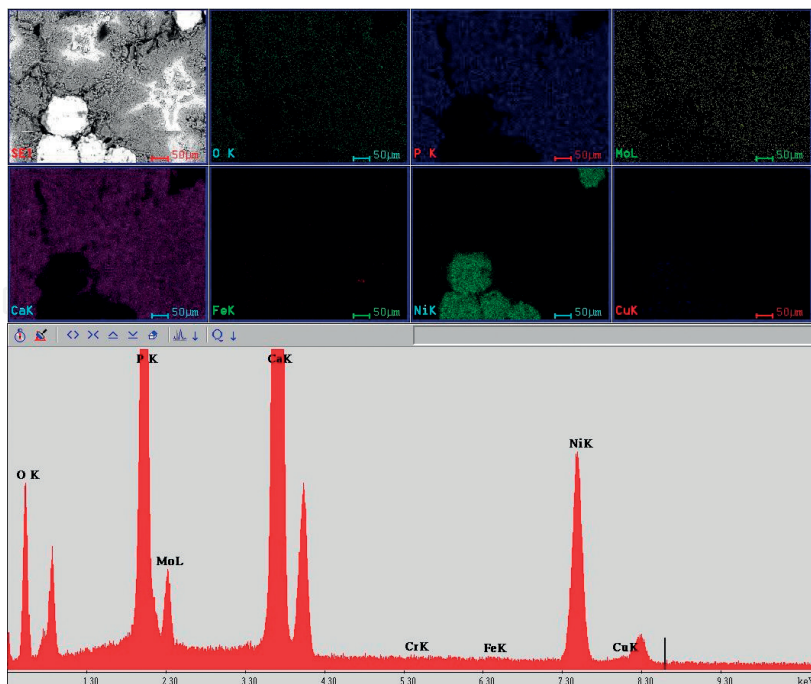


Figure 9. EDAX analysis for 70% 316L and 30% HAp composite.

3.1.4. HAp:316L composite (80%316L:20% HAp)

By a similar procedure, 80% 316L stainless steel powder and 20% of hydroxyapatite have been mixed. Two cylindrical composite with the dimensions, $\phi = 10$ mm and $h = 13$ mm, have been obtained. Composites obtained by mixing proportions of 80% 316L and 20% HAp powder are shown in **Figure 10**.

Figure 10 presents SEM microstructure of the 80% 316L and 20% HAp composite (images taken at 200 \times magnification). From microscopic analysis of the composite can be seen that the steel powder is the party round, slightly dendritic, white color. For these powder mixtures 80/20 were chosen fractions larger than 160 μm for 316L stainless steel powder and more than 45 μm for hydroxyapatite.



Figure 10. Composite image with 80% 316L and 20% HAp.

EDAX analysis of 80% 316 and 20% HAp composite shown in **Figure 11** gives us the qualitative analysis of diffusion elements present in the composite. The diagram reveals the presence of phosphorus and calcium from hydroxyapatite and the presence of specific metal elements such as Ni, Cu, Cr, Fe, and Mo elements present in stainless steel 316L.

From all elements present in the chemical composition of 316L stainless steel, there is a moderate but uniform distribution of Fe and a reduced distribution of Ni. Distribution of Cu atoms is relatively uniform but stronger in specific areas of steel metal pellets.

3.1.5. Shore hardness determination

Shore D hardness (HSD) is a dynamic feature and represents an amount proportional to the ratio of the height at which jumps back and the height from which the material was dropped through a vertical guide. To determine hardness, composites are made by powder mixtures of 70% 316L:30%HAp and 80% 316L:20% HAp.

With the help of conversion tables, the Shore hardness values measured for both types of composites have been converted to HRC and HV values, as can be seen in **Table 1**.

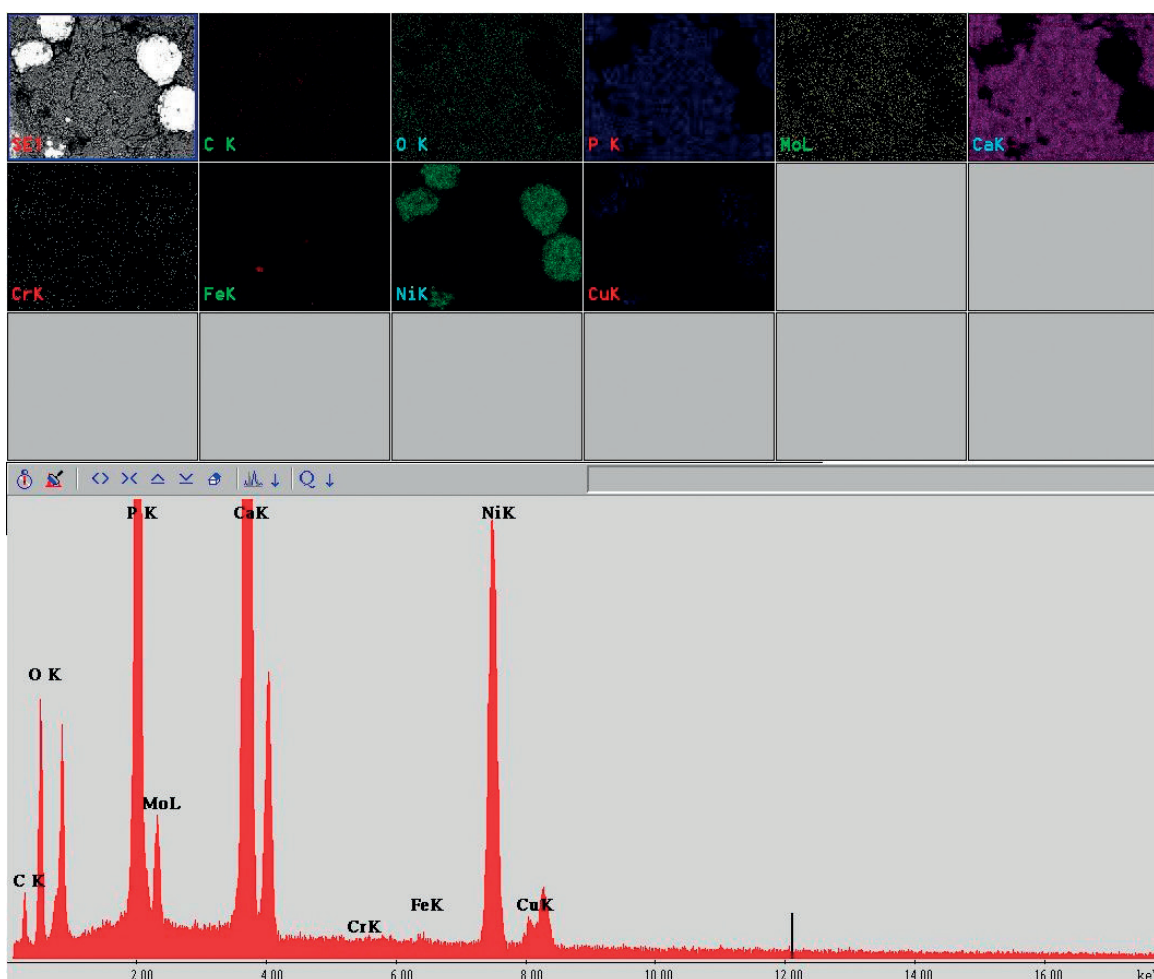


Figure 11. EDAX analysis for 80% 316L and 20% HAp composite.

No.	Composite	HSD	HRC	HV
1	70% 316L:30% HAp	71	53	560
2	80% 316L:20% HAp	77	57	643

Table 1. Composite hardness ratios with 30 and 20% HAp.

3.2. Hydroxyapatite coating of 316L stainless steel

A synthetic hydroxyapatite film obtained by sol-gel has been deposited on 316L stainless steel metal substrate, and the samples were subjected to X-ray diffraction analysis and structurally characterized by scanning electron microscopy. With this analysis the phases present in hydroxyapatite layer, morphology, and structure of hydroxyapatite were identified [24–27].

Structural quality of layers deposited by sol-gel was investigated by X-ray diffraction (XRD) analysis and scanning electron microscope (SEM) to highlight the crystallinity of deposited layers and the phases present in the hydroxyapatite film [4, 28, 29].

Figures 12 and 13(a, b) show SEM images of hydroxyapatite layer deposited on 316L stainless steel. SEM photographies reveal the existence of a layer with a thickness about 350–500 nm and with an aspect of continuous film crack with a roughness of approximately zero [30, 31].

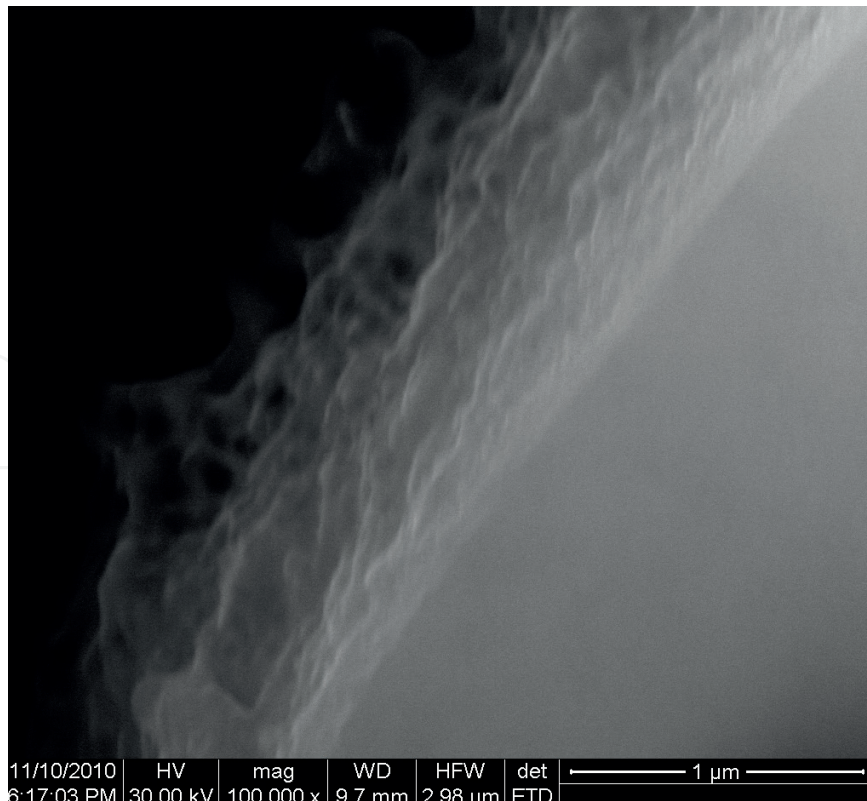


Figure 12. Film thickness of HAp deposited on 316L stainless (400,000×).

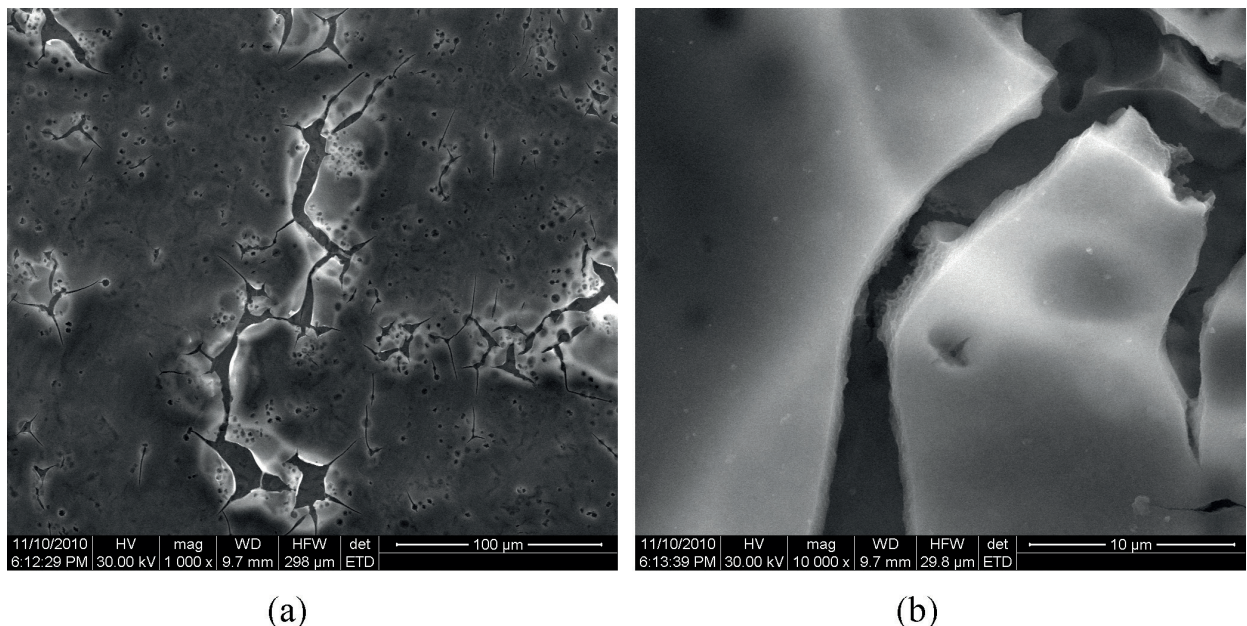


Figure 13. SEM film of HAp (500 \times) (a) and SEM film of HAp (500 \times) (b).

Appearance of the two images reveals the presence of cracks due to burning contraction between steel and hydroxyapatite layer. SEM image of the first layer of HAp is shown in **Figure 14(a)** with 2500 \times magnification.

Appearance of the second layer of hydroxyapatite on 316L stainless steel support is shown in **Figure 14(b)** at 50,000 \times magnification. Phase analysis was performed on hydroxyapatite layer deposited on the metal by using X-ray diffraction (XRD) (**Figure 15**).

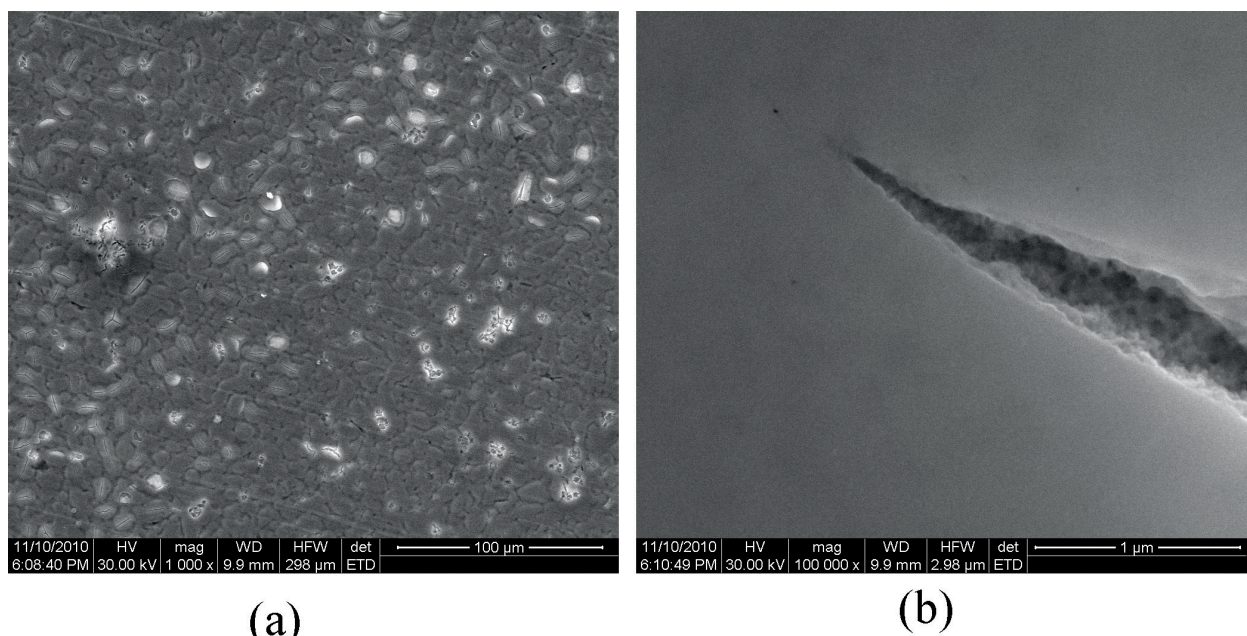


Figure 14. SEM film of HAp on oxidized steel (2500 \times) (left) and SEM image of the second film (50,000 \times) (right).

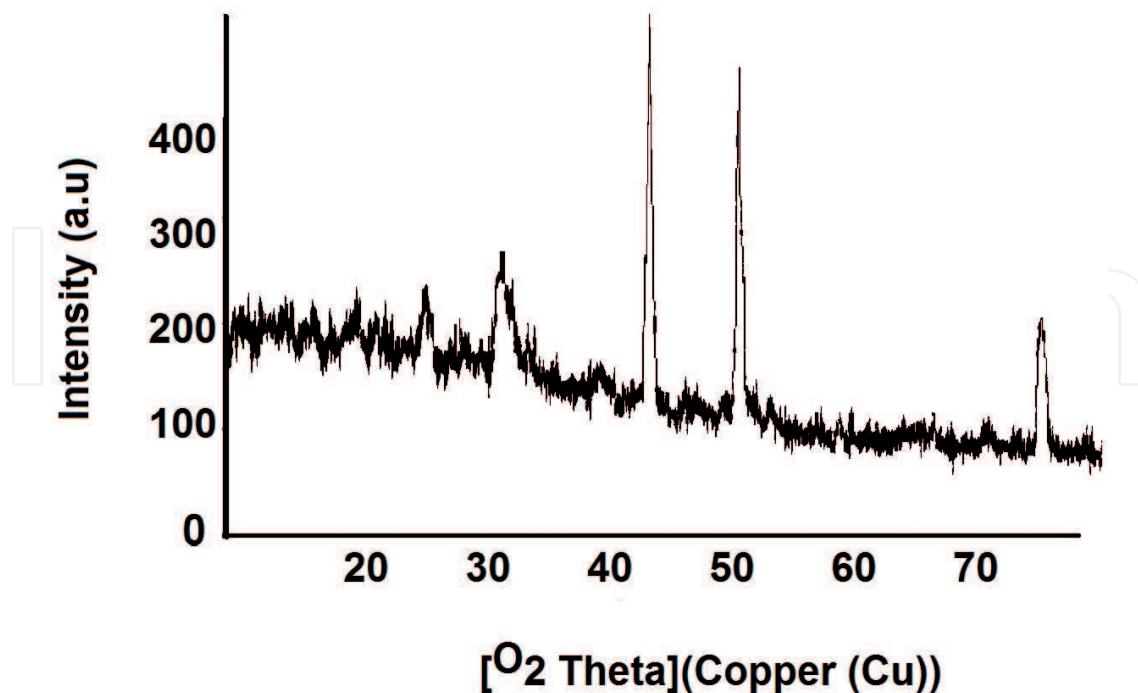


Figure 15. XRD diagram for hydroxyapatite layer deposited on the metal.

The only phase identified in the film deposited on 316L stainless steel substrate was hydroxyapatite. This method allows a good control of composition and crystallization of hydroxyapatite films at low temperatures [32, 33].

4. Behavior of the biomaterials in simulated physiological liquids

4.1. Determination of Fe, Mn, Ni, and Cr in saline and plasma by atomic absorption spectrometry

Stainless steel in medical applications is type 316 (AISI). In the 1950s, the amount of carbon in the type 316 was reduced from 0.08 to 0.03% by weight for a higher corrosion resistance in chlorides. This new alloy was known as the 316L. Even so, the use of austenitic stainless steels is limited due to the release of corrosion products in the form of Ni^{2+} , Cr^{3+} , and Cr^{6+} , which produce local effects in the body and destroy the implant [34].

For hydroxyapatite coating achieved by sol-gel method, two samples of 316L stainless steel sheet metal with 0.35 mm thickness with $15 \times 15 \times 0.35$ mm dimensions were chosen. These samples were polished with metallographic papers 400 or electrochemically attacked with 5% perchloric acid in ethanol and then were washed and dried.

The relevant metal concentration that may be released from composite materials in plasma/serum, under controlled conditions in the ppbs, has not been reported too much in the literature; for the systems created and investigated in this chapter, the metal levels in plasma/serum have been analyzed by atomic absorption spectrometry and graphite furnace technique [35, 36].

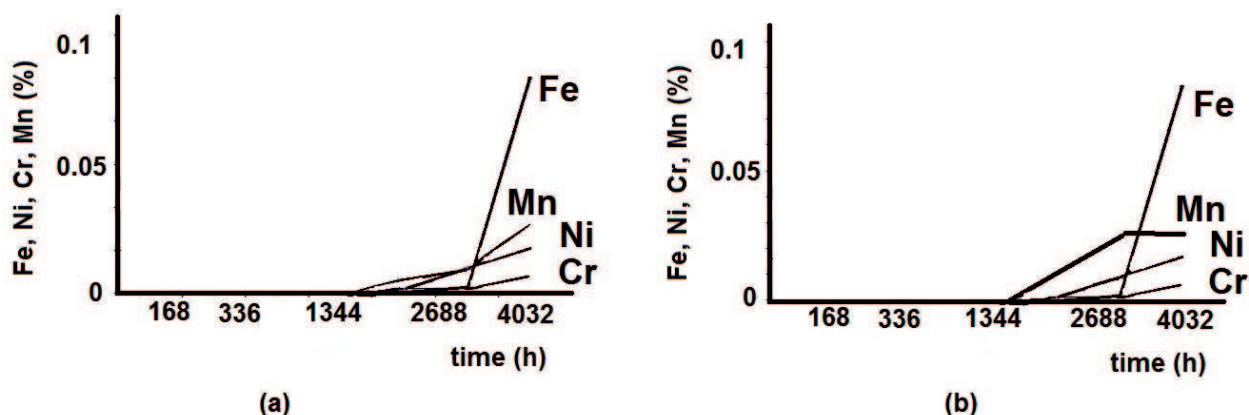


Figure 16. Changes in concentrations of Fe, Ni, Cr, and Mn in different samples.

Changes in concentrations of heavy metals like Fe, Ni, Cr, and Mn for the representative samples are plotted in **Figure 16** for two representative samples. These samples were chosen due to their higher surface exposure. Could be observed that after 6 months, the concentration of the metals (Fe, Mn, Cr, and Ni) (ppb) that may be released in simulated physiological fluids (SBF) from the used composite materials is practically zero.

The obtained results indicated that deposition of hydroxyapatite film on 316L metal plate was designed to prevent the release of metal ions in artificial plasma and in saline solution [37, 38]. **Figure 16a** presents changes in concentrations of Fe, Ni, Cr, and Mn in artificial plasma solution and in **Figure 16b** changes in concentrations of metals in saline solution.

5. Conclusions

In this chapter, the size and microscopic characterization was performed both for stainless steel powders and for hydroxyapatite and their composite. As compactness, the best compositions have been observed for 80% HAp: 20% 316L and 70% HAp: 30% 316L. The macroscopic analysis on composites with 80% HAp and 20% 316L obtained by cold pressing reveals friable samples with high porosity. It was found that:

- By increasing the amount of HAp in the composite, a lower hardness and a lower relative density for 316L/HAp composite, but with a significant increase in porosity, could be obtained.
- By increasing the proportion of HAp, the hardness or densification of the sintered composite is strongly affected.

The best mechanical results were obtained for composites of 70% 316L/30% HAp and 80% 316L/HAp 20%. Mechanical behavior studies of composites obtained were performed by analysis of Shore hardness, values of 71 HSD for composite with 70% 316L/30% HAp and 77HSD for composite with 80% 316/20% HAp. According to literature, for hydroxyapatite shore, the hardness values are between 81 and 88 HSD, and for human bones from 85 to 95 HSD. The results presented suggest that the composites obtained can be varied by choosing an appropriate chemical composition powder mixture.

The influence of grain size on the microstructure of the composite is very important because large granulations of powder will create large intergranular pores, which are affecting the density and mechanical properties of composites. HA_p powder density proportional affects the product density (HA_p/316L), so that a high density of particles will lead to a better packing density of compacted product.

In this chapter, compositional and structural investigations for composites have been established, and some correlations between the parameters of the process of preparation, chemical composition, structure, and properties of composites have been obtained, too. A comparison between composites and sol-gel coating is discussed, too.

Acknowledgements

For this chapter the authors received a financial support from UEFISCDI-MEN through the projects PNII 185/2014, PNIII 120 BG/2016, and PN 16.31.02.04.04.

Author details

Aurora Anca Poinescu¹ and Rodica-Mariana Ion^{1,2*}

*Address all correspondence to: rodica_ion2000@yahoo.co.uk

1 Materials Engineering Department, Valahia University, Targoviste, Romania

2 ICECHIM, Nanomedicine Research Group, Bucharest, Romania

References

- [1] Park JB, Bronzino JD. Metallic biomaterials. In: Taylor Print, editor. Park JB. Biomaterials: Principles and Applications. Boca Raton, London, New York, Washington, D.C.: CRC Press; 2013
- [2] BomBac D, Brojan M, FajFar P, Kosel F, Turk R. Review of materials in medical applications. RMZ-Materials and Geoenvironment. 2007;54(4):471-499
- [3] Marchant RE, Wang I. Physical and chemical aspects of biomaterials used in humans. In: Implantation Biology: The Host Response and Biomedical Devices. 1994. p. 13-38
- [4] Fan X, Chen J, Zou J, Wan Q, Zhou Z, Ruan J. Bone-like apatite formation on HA/316L stainless steel composite surface in simulated body. Transactions of Nonferrous Metals Society of China. 2009;19:347-352
- [5] Ruan JM, Zou JP, Zhou ZC. Hydroxyapatite-316L stainless steel fibre composite biomaterials fabricated by hot pressing. Powder Metallurgy. 2006;49(1):62-65

- [6] Poinescu AA, Ion RM, Van Staden RI. Different microscopic characterization techniques on hydroxyapatite powder. *Journal of Optoelectronics and Advanced Materials*. 2011;13(2-4):416-421
- [7] Monmaturapoj N. Nano-size hydroxyapatite powders preparation by wet-chemical precipitation route. *Journal of Metals Materials and Minerals*. 2008;18(1):15-20
- [8] Sung YM, Shin YK, Ryu JJ. Preparation of hydroxyapatite/zirconia bioceramic nanocomposites for orthopaedic and dental prosthesis applications. *Nanotechnology*. 2007;18:65602-65607
- [9] Poinescu AA, Ion RM, Trandafir I, Bacalum E, Radovici C. Obtaining and Characterization of a Calcium HA. In: Proc.TEHNOMUS XV "New Technologies and products in machine manufacturing technologies"; 2009. p. 301-306
- [10] Poinescu AA, Ion RM, Van Staden RI. Proceedings of SPIE-the International Society for Optical Engineering, investigations on hydroxyapatite powder obtained by wet precipitation. In: SPIE - the International Society for Optical Engineering. Advanced topics in optoelectronics, microelectronics, and nanotechnologies V; August 2010; Constanta, Romania. 2010. p. 78210B1-78210B6
- [11] Słosarczyk A, Paszkiewicz Z, Paluszakiewicz C. FTIR and XRD evaluation of carbonated hydroxyapatite powders synthesized by wet methods. *Journal of Molecular Structure*. 2005;744-747:657-661
- [12] Sahin E. Synthesis and characterization of hydroxyapatite-alumina-zirconia biocomposites [thesis], Izmir; 2006. p. 75
- [13] Ciobanu CS, Andronescu E, Stoicu A, Florea O, Le Coustumer P, Galaup S, Djouadi A. Influence of annealing treatment of nano-hydroxyapatite bioceramics on the vibrational properties. *Digest Journal of Nanomaterials and Biostructures*. 2011;6(2):609-624
- [14] Donadel K, Laranjeira CMM, Gonçalves VL, Favere VT, De Lima JC, Prates LHM. Hydroxyapatite produced by wet-chemical methods. *Journal of the American Ceramic Society*. 2005;88(8):3374-3374
- [15] Cengiz B, Gokce Y, Yildiz N, Aktas Z, Calimli A. Synthesis and characterization of hydroxyapatite nanoparticles. *Colloids and Surfaces A: Physicochemical and Engineering Aspects*. 2008;322(1-3):29-33
- [16] Rintoul L, Wentrup-Byrne E, Suzuki S, Grøndahl L. FT-IR spectroscopy of fluoro-substituted hydroxyapatite: Strengths and limitations. *Journal of Materials Science. Materials in Medicine*. 2007;18(9):1701-1709
- [17] Rehman I, Bonfield W. Characterization of hydroxyapatite and carbonated apatite by photo acoustic FTIR spectroscopy. *Journal of Materials Science. Materials in Medicine*. 1997;8(1):1-4
- [18] Boanini E, Bigi A. Biomimetic synthesis of carbonated hydroxyapatite thin films. *Thin Solid Films*. 2006;497:53-57

- [19] Bogza ES. Studii cinetice și de echilibru ale unor procese de reținere pe materiale apatitice [thesis]. Cluj Napoca; 2010
- [20] Poinescu AA, Ion RM. Particles dimensional analysis and microscopic characterization of hydroxyapatite powder. In: TEHNOMUS—New Technologies and Products in Machine Manufacturing Technologies; 2011; Suceava. Suceava: Universitatea "Stefan Cel Mare", Suceava; 2011. p. 283-288
- [21] Chai C, Ben-Nissan B. Thermal stability of synthetic hydroxyapatites. International Ceramic Monographs. 1994;1(1):79-85
- [22] Chai CS, Ben-Nissan B. Bioactive nanocrystalline sol-gel hydroxyapatite, coatings. Journal of Materials Science. Materials in Medicine. 1999;10:465-469
- [23] Anderson D, Hastings GW, Morrey S, Rich C, Hydroxyapatite ceramic coatings. In: Heimke G, editor. Bioceramics, vol 2. Proceedings of the 2th International Symposium on Ceramics in Medicine; Heidelberg: 1989. p. 251
- [24] Berndt CC, Haddad GN, Gross KA. Thermal spraying for bioceramics application. In: Heimke G, editor. Proceedings of the 2th International Symposium on Ceramics in Medicine; Heidelberg: 1989. p. 201
- [25] Ben-Nissan B, Milev A, Vago R. Morphology of sol-gel derived nano-coated coralline hydroxyapatite. Biomaterials. 2004;25:4971-4975
- [26] Ion RM. Nanocrystalline Materials. Bucharest: FMR; 2003. 189 p
- [27] Poinescu AA, Radulescu C, Vasile BS, Ionita I. Research regarding sol-gel hydroxyapatite coating on 316L stainless steel. Revista de Chimie. 2014;65(10):1245-1248
- [28] Ballarre O, Liu Y, Mendoza E, Schell H, Diaz F, Orellano JC, Fratzl P, Ceré S. Enhancing low cost stainless-steel implants: Bioactive silica-based sol-gel coatings with wollastonite particles. Journal of Nano and Biomaterials. 2012;4:33-53
- [29] Bermudez R, Espinoza Beltran FJ, Espitia Cabrera E, Contreras Garcia ME. Characterization of HA_p-ZrO₂ base bilayer on 316L stainless steel substrates for Orthopaedic prosthesis applications. Advanced in Technology of Materials and Materials Processing Journal. 2007;9(2):141-148
- [30] Cao W, Hench LL. Bioactive materials. Ceramics International. 1996;22:493-507
- [31] Miao X. Observation of microcracks formed in HA-316L composites. Materials Letters. 2003;57:1848-1185
- [32] Nayar S, Hydroxyapatite PA. Coating on stainless steel pre-coated with bovine serum albumin at ambient conditions. Colloids and Surfaces B: Biointerfaces. 2006;48:183-187
- [33] Seo DS, Kim YG, Hwang KH, lee JK. Preparation of hydroxyapatite powder derived from tuna bone and its sintering property. Journal of the Korean Ceramic Society. 2008;45(10):594-600

- [34] Balamurugan A, Balossier G, Kannan S, Michel J, Faure J, Rajeswari S. Electrochemical and structural characterisation of zirconia reinforced hydroxyapatite bio ceramic sol-gel coatings on surgical grade 316L SS for biomedical applications. *Ceramics International*. 2007;**33**:605-614
- [35] Wataha JC, Nelson SK, Lockwood PE. Elemental release from dental casting alloys into biological media with and without protein. *Dental Materials*. 2011;**17**:409-415
- [36] Williams DF. *The Williams Dictionary of Biomaterials*. 1st ed. Liverpool: Liverpool University Press; 1999
- [37] Aizawa T, Kaneko T, Yajima H, Yamada S, Sato Y, Kanda Y, Kanda S, Noda M, Kadokawa T, Nagai M, Yamauchi K, Komatsu M, Hashizume K. Rapid oscillation of insulin release by the rat pancreatic islets under stringent Ca^{2+} -free conditions. *The Journal of Endocrinology*. 2000;**166**:545-551
- [38] Poinescu AA, Ion RM, Stan R, Rizescu CZ. Determining sensitivity to intergranular corrosion of austenitic stainless steel 316L. *The Scientific Bulletin of Valahia University-Materials and Mechanics*. 2010;**5**(8):91-94

